Measurement of the electron yield of CsI with polarized x rays

S. Hanany, P. S. Shaw, Y. Liu, A. Santangelo,* P. Kaaret, and R. Novick
Department of Physics, Columbia University, New York, New York 10027
(Received 21 May 1992; revised manuscript received 11 December 1992)

We investigate the polarization dependence of photoemission from polycrystalline CsI under excitation by linearly polarized 2.69-keV x rays. We measure the electron pulse yield as a function of polarization state for grazing incidence angles between 5° and 18°. No dependence on the incident polarization is found. We find an upper limit of 1.1%, at the 99.99% statistical confidence level, on the fractional change in the pulse yield. Allowing for worst-case systematic uncertainties, we place an upper bound of 3.6% on the difference in the *secondary* electron pulse yield between the two polarization states.

I. INTRODUCTION

The energy spectrum of electrons emitted from a solid after excitation with x rays consists of the primary and Auger electrons and of a large number of low-energy electrons (energy less than ~ 50 eV). These low-energy electrons, which typically comprise more than 50% of the total number of electrons emitted, are sometimes referred to as "true secondary" electrons. The true secondary electrons are believed to be the product of inelastic collisions of the primary and Auger electrons with other electrons in the solid. In some materials the electronic emission is dominated by the secondary electrons. With CsI, secondary electrons constitute more than 99% of the total number of emitted electrons.[1]

Following an excitation by an impinging x-ray photon (or a charged particle with sufficient energy), usually more than one electron is ejected from the photocathode surface.[2] Thus electron yield measurements are conducted either in a pulse yield mode[3] or in a current yield mode.[1,4] In a pulse yield measurement each absorption of a photon which leads to an emission of an electron or electrons, i.e., each "emission event," is recorded as a single count. Thus pulse yield can be defined as the number of emission events per incident photon. The total (or current) yield is defined as the average number of electrons emitted from the photocathode per incident (or sometimes, absorbed) photon. (In a total yield measurement one records the current leaving the surface as a function of the number of incident, or absorbed, photons.) In terms of a set of quantities p_n $(n=0,1,\ldots)$, which give the probability that n electrons will be emitted per incident photon, the pulse yield Y_P is given by

$$Y_P = 1 - p_0 \tag{1}$$

and the total yield Y_C is given by

$$Y_C = \bar{n} = \sum_{n=1}^{n=\infty} n p_n \ . \tag{2}$$

The total yield, and to some extent the pulse yield, of different materials following an excitation by either photons or charged particles have been investigated in the past.[1,3,4] In particular, the dependence of the current yield on the linear polarization of the incident optical and near-UV radiation has become known as the vectorial photoelectric effect[5-12] and theories which account for the surface and bulk contributions to the observed vectorial effect have been developed.[13,14]

Very few experiments have studied the dependence of either the total yield or the pulse yield on polarized exciting radiation in the soft x ray or extreme ultraviolet (EUV) bands.[15,16] It is only recently that more experiments were conducted.[17-19] These were motivated by a possible application to polarimetry in x-ray astronomy.[17,20] The experiments, conducted with CsI and other polycrystalline photocathodes, were reported to show that the electron total and pulse yields of photocathodes irradiated with linearly polarized EUV or soft x-ray photons depend strongly on the polarization state of the incident beam.[17-19] This is a surprising result since it implies that the polarization information contained in the beam survives the various processes between the creation of a high-energy photoelectron, which is liberated from an atomic core level, and the eventual escape of primarily low-energy secondary electrons from the photocathode. This is in contrast to photoemission following excitation with optical and near-UV radiation where the electron yield is dominated by primary electrons, which are emitted from the valence and conduction bands.

To the best of our knowledge, there are no theoretical models which explicitly relate either the total yield, or the pulse yield, or the probabilities p_n, to the polarization of the incident x rays.

In this paper we present the results of experiments in which we investigate the dependence of the pulse yield Y_P of a polycrystalline CsI photocathode as a function of the polarization state of 2.69-keV x rays.

We separate the contributions to Y_p to events which contain low-energy secondary electrons and to events which contain only high-energy electrons, and we place an upper bound on the difference in the secondary electron-pulse yield between the two polarization states. Our results are in conflict with previously reported experimental measurements.[17,19,21] We discuss the disparity between the experiments.

II. EXPERIMENTAL SETUP

The experimental setup is shown in Fig. 1. It consisted of an x-ray source, a Bragg crystal, a photocathode, and an electron detector. The whole system was maintained at a pressure of about 10^{-6} Torr.

The rhodium anode of the x-ray source was kept at a voltage higher than 3 kV in order to excite the rhodium $L_{\alpha_1}=2.697$-keV and $L_{\alpha_2}=2.692$-keV lines. A 25 μm thick beryllium filter, located between the x-ray source and the Bragg crystal, attenuated the UV component of the beam, and a Si(111) crystal oriented at a Bragg angle of 47.2° attenuated beam components other than 2.69-keV x rays which satisfy the Bragg condition for this Bragg angle. The combined contribution of beam components other than the Bragg selected 2.69-keV x rays (i.e., Bragg reflected continuum radiation from the source, fluorescence from the Si crystal or from the Be filter, UV radiation) was found to be less than 0.5% of the total detector count rate. Because the Bragg angle is close to 45° the silicon Bragg crystal also polarized the beam. The polarization of the beam was measured and was found to be more than 90%. For alignment purposes, two additional collimators were mounted in the main chamber between the Bragg crystal and the photocathode-detector assembly.

The photocathode and the photoelectron detector assembly (shown in Fig. 2) were mounted in the main chamber so that x rays reflected from the Bragg crystal impinge on the flat photocathode at an adjustable grazing incidence angle θ. The experiments were conducted at low grazing incidence angles ($<20°$) because previous experiments were reported to demonstrate that the dependence of the pulse yield on the polarization of the beam increased with decreasing grazing incidence angle below $\sim 25°$. The assembly could also be rotated in the ϕ direction (around the z axis). This rotation changes the orientation of the photocathode with respect to the polarization vector of the beam. Electrons emitted from the photocathode were focused into and then detected by a microchannel plate (MCP) detector. The MCP detector consisted of two resistance matched microchannel plates under a potential drop of 2000 V (total over both plates). The typical MCP background count rate was less than five counts/s.

The charge pulse generated by the MCP was amplified by a charge sensitive preamplifier and then routed to a standard pulse counting system which consisted of a shaping amplifier, a single-channel analyzer, and a counter. We also used a multichannel analyzer for pulse-height analysis. The pulse height is approximately proportional to the number of electrons that enter the MCP and initiate the pulse (the full width at half maximum of the pulse-height distribution was about 100%).

To achieve maximal collection of the electrons we found it crucial to use an electrostatic focusing system. This is first because an appreciable fraction of the electrons may be emitted in directions away from the entrance aperture of the detector. Second, at small grazing incidence angles the x-ray beam is spread over an area on the photocathode whose size is on the order of $d_x(d_y/\sin\theta)$, where d_x and d_y are the dimensions of the cross section of the beam. Hence electrons may be emitted relatively far from the detector's center axis. We note that incomplete collection of the electrons emitted from the photocathode may bring about serious systematic effects. In the Appendix we demonstrate how such spurious effects arise.

The electron focusing system consisted of a "field forming" ring, and two metal grids (see Fig. 2). In a typical data collection configuration, the field forming ring and the photocathode were grounded, grid No. 1 was maintained at +460 V, grid No. 2 at +480 V, and the entrance aperture to the MCP was kept at +500 V.

The electrostatic lens was designed to focus electrons of energy $E_e \lesssim 15$ eV. Henke, Knauer, and Premaratne[1] investigated the energy distribution of secondary electrons, and the ratio between the number of secondary and primary electrons emitted from the surface of a polycrystalline CsI photocathode excited with soft x rays ("primary" here means electrons of energy more than 50 eV). They found that more than 99.5% of the secondaries emitted from a 3000 Å thick CsI photocathode have energies below 5 eV. Because of the high secondary yield of CsI, these secondaries constitute more than 99% of the total number of electrons emitted from the photocathode surface.

Computer simulations[22] of the electrostatic focusing system show that all electrons of energies less than 5 eV

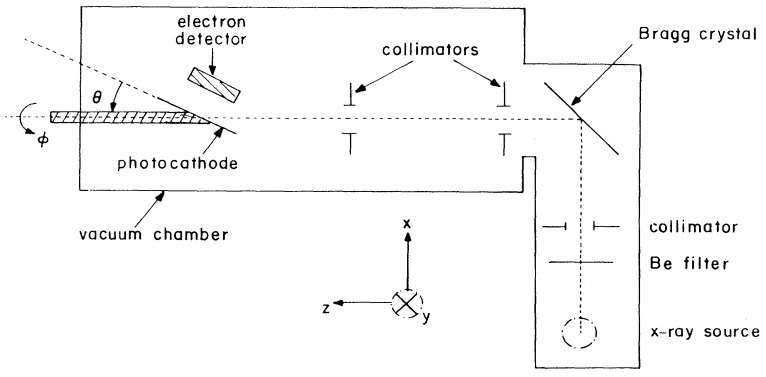

FIG. 1. The experimental setup.

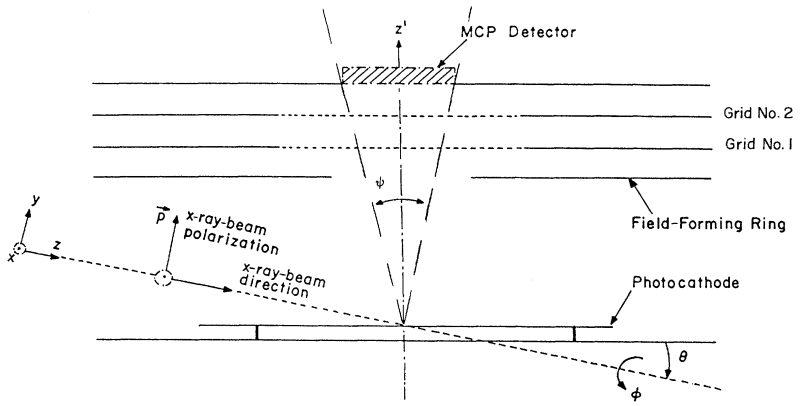

FIG. 2. Detector and photocathode assembly.

that are emitted from the photocathode within a radius of 21 mm from the symmetry axis of the detector, at polar angles less than 80°, measured from the normal to the surface, will be focused into the detector. We have also obtained experimental evidence which indicates that to an accuracy of 0.5% all the emission events which contain secondary electrons were recorded by the MCP detector at both the σ and π polarization states. [In a π (σ) state the polarization vector is in (perpendicular to) the plane of incidence.] We describe these measurements in the Appendix.

A magnetic field of 0.4 G was measured between the photocathode and the detector. Such a field can be shown to have a negligible effect on the count rates.

The photocathode consisted of 3000 Å CsI (more than 99.99% pure) deposited on a polished three inch diameter Si(100) wafer by thermal evaporation. Typical evaporation rates were about 10 Å/s. The thickness was monitored with a quartz-crystal film thickness monitor. A photocathode thickness of 3000 Å was chosen because the escape depth for electrons in CsI is about 250 Å (Refs. 1 and 23) and the photoelectric yield depends on the material thickness up to about 1500 Å.

The evaporation took place in a separate vacuum chamber, under a pressure of about 10^{-6} Torr. The photocathodes were exposed to atmospheric conditions for about 15 min during their transfer to the main vacuum chamber. A CsI sample photocathode that had the same exposure to atmospheric conditions was subjected to x-ray photoelectron spectroscopy and to Auger electron spectroscopy studies. We found that less than 5% in atomic concentration of oxygen and carbon were adsorbed on the surface. This is consistent with the data of Premaratne *et al.*[24] who showed that the x-ray quantum yield of vacuum-evaporated CsI photocathodes that were exposed to air (63% relative humidity) for a duration of 30 min did not change by more than 4%, and that the energy distribution of the secondary electrons did not show any significant change even after a three hour exposure. Scanning electron microscope pictures of the surface show grains with sizes of up to 1 μm. Similar structure is reported by Fraser, Lees, and Pearson[17] and Chappel, Everman, and Murray[25] (Chappel, Everman, and Murray report that evaporated CsI forms in pillarlike structures and that the observed grains are the tops of these pillars).

Reproducibility of the results was checked by repeating the measurements with different photocathodes, with varying exposure times to atmospheric conditions (from a few minutes up to about an hour), and upon reorientation of the photocathodes (to test for the effects of surface nonuniformities). The same results were obtained at all configurations.

III. MEASUREMENTS AND ANALYSIS

A. Measurement procedure

The data consists of "rotation curves" measured at five different grazing incidence angles. In a rotation curve we record the count rate as a function of the rotation angle ϕ of the photocathode (see Figs. 1 and 2). Measurements were taken every 5°.

We also measured background rotation curves by blocking the beam just before the sample. Signal to background ratios depend on the grazing incidence angle. Typically, the values are 50 for a grazing incidence angle of 18°, and larger than 100 for a grazing incidence angle of 5°. In what follows it should be understood that any background contribution to the signal was measured and subtracted from it.

Pulse-height distributions of the signal and the background were recorded at only the σ and π polarization states at incidence angles of 10° and 15°.

B. Analysis of the rotation curves

In the absence of background or spurious modulation effects we can write the expected signal as

$$S(\phi)=S_0+A\cos[2(\phi+\phi_0)]\ , \tag{3}$$

where S_0 is the average count rate and ϕ is the rotation angle of the plane of incidence measured with respect to the polarization vector. We choose $\phi=0°$ to correspond to a π state and A is taken to be positive. The presence of the phase ϕ_0 is motivated first because the modulation factor, as defined below, is a positive definite quantity which contains information about the relative yields between the σ and π polarization states only when used together with ϕ_0. Second, earlier experiments[17,21] indicated

that the modulation curve exhibits a "phase shift;" that is, the maximum and minimum of the counting rates did not coincide with the beam being at either a σ state or a π state (in other words ϕ_0 was different from 0° or 90°). The implication of the existence of a phase shift are further discussed in Sec. V.

We define the modulation factor and the phase associated with the measured data in a manner analogous to polarization analysis (note that this is slightly different than the definition which appears in Refs. 17 and 19). We write the signal as

$$S(\phi)=S_0+A_1\cos(2\phi)+A_2\sin(2\phi)\ , \tag{4}$$

with

$$A_1=A\cos(2\phi_0) \tag{5}$$

and

$$A_2=-A\sin(2\phi_0)\ . \tag{6}$$

We now define two components of the modulation factor

$$M_1=\frac{A_1}{S_0} \tag{7}$$

and

$$M_2=\frac{A_2}{S_0}\ , \tag{8}$$

and we define the modulation factor as

$$M=\sqrt{M_1^2+M_2^2}\ . \tag{9}$$

The phase is given by

$$\phi_0=0.5\arctan\left[-\frac{A_2}{A_1}\right]=0.5\arctan\left[-\frac{M_2}{M_1}\right]\ . \tag{10}$$

The modulation factor defined in this way is a generalization of the modulation factor, denoted here M', that was used in some previous works.[17,19] M' was defined as

$$M'=\frac{S(\sigma)-S(\pi)}{S(\sigma)+S(\pi)}\ , \tag{11}$$

where $S(\sigma)$ and $S(\pi)$ are the count rates recorded at σ and π polarization states, respectively. The phase ϕ_0 was not considered when calculating the modulation factor, or it was implicitly assumed to vanish or equal 90°. M' was positive or negative depending on whether $S(\sigma)$ was larger or smaller than $S(\pi)$. In the current formulation M is always positive, and

$$M=|M'|=\frac{|S(\sigma)-S(\pi)|}{S(\sigma)+S(\pi)} \tag{12}$$

only when $\phi_0=0°$ or 90°.

In order to extract modulation factors from the measured rotation curves we least squares fitted each modulation curve with a function of the form

$$f=a_0+a_1\cos(\phi)+a_2\sin(\phi)+a_3\cos(2\phi)+a_4\sin(2\phi)\ . \tag{13}$$

The terms varying sinusoidally with a ϕ dependence (as contrasted with a 2ϕ dependence) were introduced in order to account for a possible variation in the quantum efficiency of the photocathode. The quantum efficiency depends on ϕ if the x-ray beam is not properly aligned with the axis of rotation of the photocathode-detector assembly (such systematic effects are discussed in more detail elsewhere[26,29]). Given such a fit, we find the two components of the modulation

$$M_1=\frac{a_3}{a_0} \tag{14}$$

and

$$M_2=\frac{a_4}{a_0}\ , \tag{15}$$

and the modulation factor and the phase are given by Eqs. (9) and (10). A measure of how well Eq. (13) fits the experimental data is obtained by calculating the χ^2 statistic and then finding the probability that such a value, or larger, should occur by chance.

A convenient way to present both the modulation factor and the phase is by means of a "modulation factor polar plot" whose radial axis is the modulation factor M and the phase ϕ_0 is given in the azimuthal direction. On each polar plot we also show two contours which correspond to the 68.3% and 99.99% statistical confidence levels. The modulation factors are given in terms of percentages from the maximum possible value, $M_{\max}=1$.

IV. RESULTS

Rotation curves were measured for the following five grazing incidence angles: $\theta=5°$, 8°, 10°, 15°, and 18°. The rotation curve and the modulation factor polar plot for $\theta=15°$ are shown in Fig. 3. Polar plots corresponding to the other incidence angles are presented in Fig. 4. Table I lists all the values of the fitted Fourier coefficients $a_{1\ldots4}$ together with the derived modulation factors and the

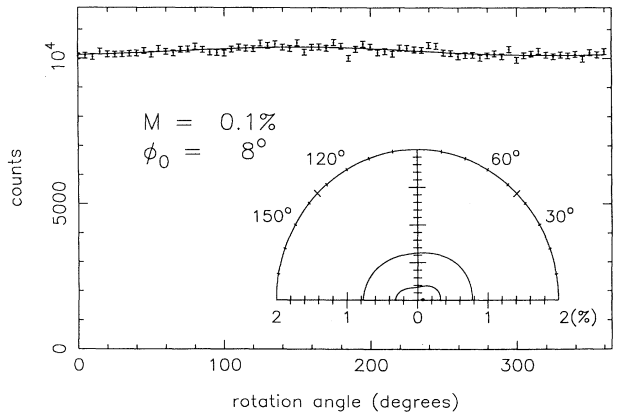

FIG. 3. Electron-pulse yield as a function of the x-ray beam polarization ("rotation curve"). The grazing incidence angle is 15°. Continuous line: A least-squares fit to the data points. We also show the modulation factor M, the phase ϕ_0, and a modulation factor polar plot. Rotation angles of 0° and 180° (90° and 270°) correspond to a π (σ) polarization state. In the polar plot, M and ϕ_0 are given in the radial and azimuthal directions, respectively. The contours correspond to the 68.3% and 99.99% statistical confidence level.

TABLE I. Results of the least-squares fitting of the experimental rotation curves. θ is the grazing incidence angle, M is the modulation factor given in percent, ϕ_0 is the phase, and q is the probability that the χ^2 statistic should obtain, by chance, a value equal to or larger than the one found for the particular fit. $a_{1\ldots4}$ are the Fourier coefficients of the fit normalized by a_0 [see Eq. (13)]. All quoted errors are a 1σ statistical confidence level. * means that any phase angle between 0° and 180° is possible at the 1σ level.

θ	M (%)	ϕ_0	q	10^3a_1	10^3a_2	10^3a_3	10^3a_4
5°	$0.01^{+0.1}_{-0.01}$	97°±*	0.61	−15.0±0.9	18.0±0.9	−0.1±0.9	0.03±0.9
8°	0.3±0.2	75°±18°	0.89	−24.0±1.2	12.1±1.2	−2.4±1.2	−1.4±1.2
10°	0.3±0.2	140°±23°	0.13	−20.4±1.3	18.3±1.3	0.5±1.3	2.7±1.3
15°	$0.08^{+0.2}_{-0.08}$	8°±*	0.36	−12.2±1.6	7.1±1.7	0.7±1.6	−0.02±1.7
18°	0.4±0.3	137°±20°	0.20	−10.5±1.8	5.6±1.8	0.3±1.8	4.0±1.8

phases. q is the probability that a value as large as, or larger than, the one obtained for the χ^2 statistic should occur by chance. The data in the table show that the modulation factors characterizing the pulse yield have values $M \leq 0.4\%$. The polar plots show that on the 99.99% confidence level the modulation factors are all consistent with null modulation and with an upper limit of 1.1%, obtained at a grazing incidence of 18°. At smaller grazing incidence angles, the upper limits are smaller due to the increase in the quantum efficiency and hence better statistics. As far as the phases are concerned, there is no apparent consistent pattern for the values of the phases as a function of incidence angle. This can be viewed as an additional indication for the absence of any statistically significant modulation factor.

Pulse-height distributions recorded at π and σ polarization states, at grazing incidence angles of 10° and 15°, are presented in Fig. 5. For a given grazing incidence angle θ we present the two polarization states for comparison.

V. DISCUSSION

A. Comparison with other experiments

Our results do not agree with previously reported measurements[17,19,21] which claimed that modulation factors larger than 10% were observed at grazing incidence angles smaller than 20°; $M \simeq 70\%$ was reported at an incidence angle of 5°.[17] Some of these experiments also indicated that a substantial difference was observed between the pulse-height distributions recorded in the σ and π polarization states.[21] We suggest that spurious systematic effects may have affected the earlier experiments. We have already mentioned, in Sec. II, the sensitivity of the experiment to such effects. In the Appendix we discuss how arbitrary modulation factors and phases can be produced if care is not taken to eliminate the sources of spurious modulation. We also argue that differences in the pulse-height distributions recorded at σ and π polarization states may arise due to the same systematic effects. We present elsewhere[26] data which demonstrate the sensitivity of both the rotation curves and the pulse-height distributions to the spurious effects.

The phase of about 20° reported in previous studies[17,21] indicates the existence of a preferred direction in the experiment in addition to the directions defined by the plane of incidence and the polarization vector. Such preferred direction can be introduced either by spurious instrumental effects, such as those discussed in the Appendix, or by a special geometry of the evaporated photocathode material. It has been suggested that the pillar-

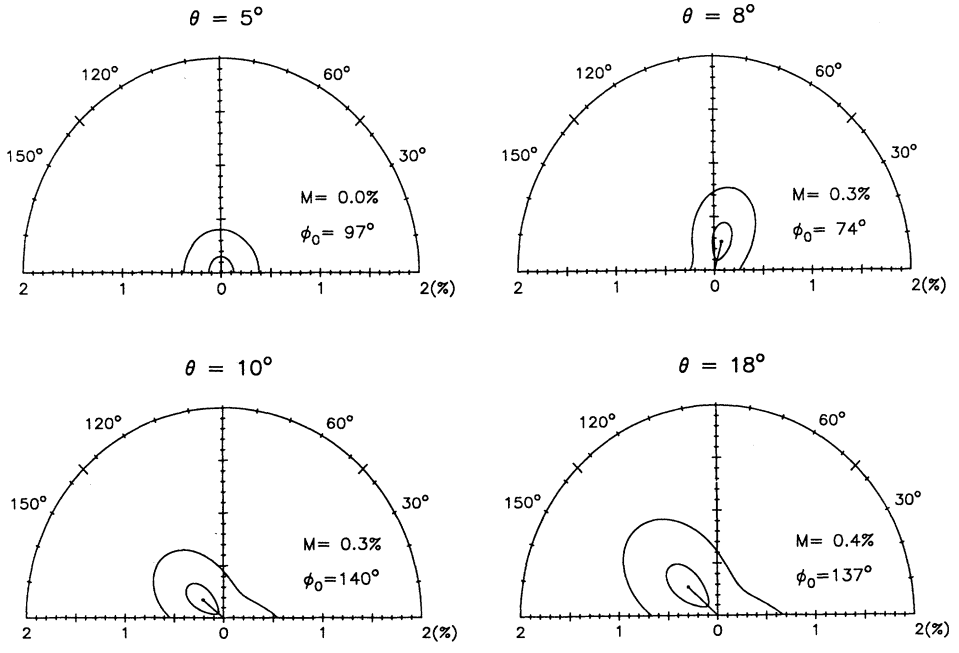

FIG. 4. Modulation factor polar plots obtained at grazing incidence angles of 5°, 8°, 10°, and 18°.

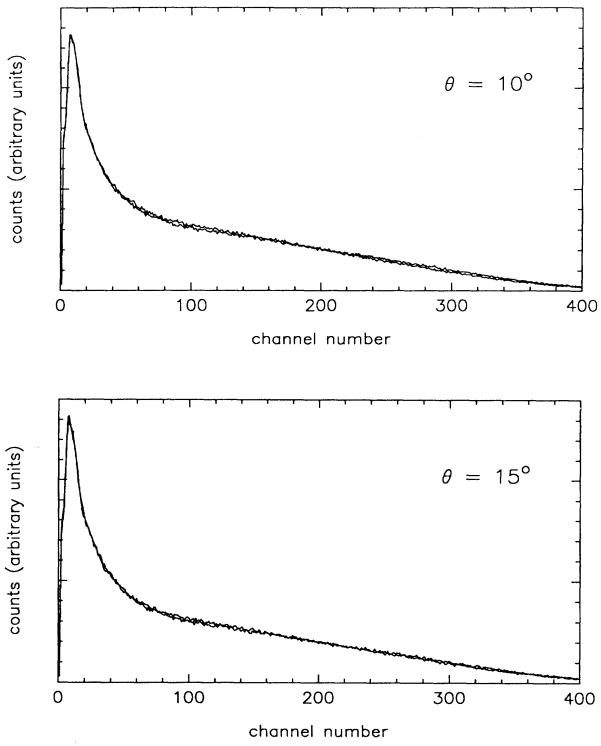

FIG. 5. Pulse-height distributions measured at grazing incidence angles of 10° and 15°. For each grazing incidence angle we show the pulse-height distributions recorded at both the π and σ polarization states.

like structure of evaporated CsI (Ref. 25) introduces the additional preferred direction.[17] If these pillars are the source of the phase shifts, then a rotation of the photocathode (around the surface normal) should change their values. In the experiment reported here no statistically significant phases, and indeed no phase shifts, were observed at any photocathode rotational position.

One of the previous experiments[17] that reported nonvanishing modulation factors was conducted with 1600 Å thick CsI evaporated on a stainless-steel substrate. We tried to reproduce the result with the same material thickness and substrate. Figure 6 shows the rotation curve and polar plot measured at an incidence angle of 10° with a 1600 Å thick CsI photocathode evaporated on a stainless-steel substrate. It shows that the modulation factor is consistent with zero at the 68.3% confidence level. On the 99.99% confidence level the upper limit obtained for grazing incidence angles between 5° and 18° is 1% (data presented in Ref. 26).

B. Polarization dependence of the secondary electron pulse yield

The total number of emission events N is given by

$$N = Y_P N_\gamma \ , \tag{16}$$

where Y_P is the pulse yield and N_γ is the number of incident photons. Since during an emission event, electrons of various energies are emitted from the photocathode, the pulse yield can be expressed as composed of contributions from different types of events. N can be written as

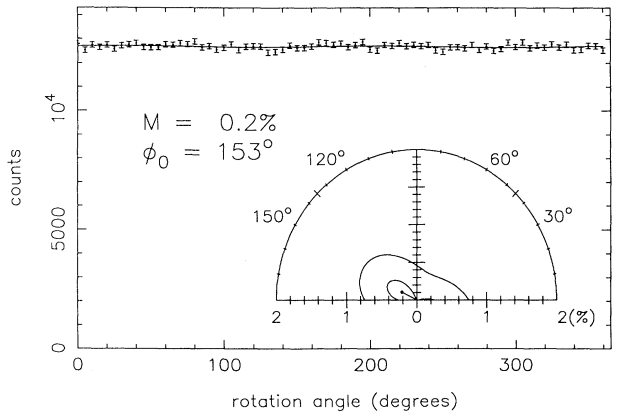

FIG. 6. Electron-pulse yield as a function of the x-ray beam polarization state measured with 1600 Å CsI evaporated on a stainless-steel substrate. The grazing incidence angle is 10°.

$$N(\phi) = N_s'(\phi) + N_p(\phi) + N_{sp}'(\phi) \ , \tag{17}$$

where N_s' is the number of events which contain only electrons with energy $E_e \leq 15$ eV, N_p is the number of events which contain only electrons with energy $E_e > 15$ eV, and N_{sp}' is the number of events which contain both low- and high-energy electrons. We choose 15 eV as a "threshold" energy because essentially all the secondary electrons emitted from CsI have energies lower than 15 eV.[1] The angle ϕ determines the polarization state of the beam.

In what follows we wish to concentrate on the dependence on polarization of the pulse yield of events which contain secondary electrons. Thus we need to look at the signal generated by N_s' and N_{sp}' together. This leads us to write the total number of emission events N as a sum of only two terms,

$$N(\phi) = N_s(\phi) + N_p(\phi) \ , \tag{18}$$

where $N_s = N_s'(\phi) + N_{sp}'(\phi)$ is the number of events which contain *at least* one electron with energy $E_e \leq 15$ eV. We note that Eq. (18) effectively separates the pulse yield Y_P to contributions from events which contain secondary electrons Y_{Ps} and to events which contain only high-energy electrons Y_{Pp}:

$$Y_P(\phi) = 1 - p_0(\phi) = Y_{Ps}(\phi) + Y_{Pp}(\phi) \ . \tag{19}$$

The electrostatic focusing system is designed to focus low-energy electrons, $E_e < 15$ eV. Primary and Auger electrons and diffused primaries will not be efficiently focused. For example, computer simulations show that the trajectories of electrons with energies larger than 250 eV will only be negligibly affected by the electrostatic fields between the photocathode and the detector. Thus, the signal S recorded by the detector can also be separated into two terms,

$$S(\phi) = S_s(\phi) + S_p(\phi) \ , \tag{20}$$

where S_s is the signal due to events which contain at least

one electron with energy $E_e \leq 15$ eV and S_p is the signal due to events which contain only electrons with energy $E_e > 15$ eV.

For low-energy electrons, $E_e \leq 15$ eV, the effective acceptance angle of the detector is close to 2π; electrons emitted in any polar angle (measured from the normal to the surface) will be focused into the detector. As stated earlier, we have established experimentally that more than 99.5% of the events that contain low-energy electrons are detected at both polarization states. Thus $S_s \simeq N_s$ and S_s measures the variation of the total number of secondary electron emission events as a function of polarization.

Electrons with energies $E_e > 15$ eV may or may not reach the detector depending on their momentum vector when emitted from the surface. Electrons with energies $E_e \gtrsim 250$ eV will only be detected if they are emitted into the solid angle subtended by the detector at the point of emission. Therefore, S_p may depend on ϕ either because the total number of emission events (that contain high-energy electrons) depends on the polarization state, or because the detector samples different parts of the angular distribution of the high-energy electrons.

Regardless of its source, both S_s and S_p may have a dependence on the polarization of the incoming x rays. We write

$$S(\phi)=S_{p0}+A_p\cos[2(\phi+\phi_p)] + S_{s0}+A_s\cos[2(\phi+\phi_s)] , \quad (21)$$

where all the quantities are defined similarly to those in Eq. (3). When $\phi_s=\phi_p$ we find that the modulation of S is given by

$$M=\frac{M_s+M_p\eta}{1+\eta} , \quad (22)$$

where $M_s(M_p)$ is the modulation factor of $S_s(S_p)$ and $\eta=S_{p0}/S_{s0}$. When $\phi_s=0°$ and $\phi_p=\pi/2$, or the reverse,

$$M=\frac{|M_s-M_p\eta|}{1+\eta} \quad (23)$$

and the phase of M is zero if $M_s-M_p\eta>0$, or $\pi/2$ if $M_s-M_p\eta<0$. The case of arbitrary phases for the signals S_s and S_p is irrelevant for what follows. Equations (22) and (23) will now be used to find an upper limit on M_s.

We first estimate η by using data about the current yield of CsI and by considering our particular experimental apparatus. We then find limits on M_s depending on the level of modulation M_p that is assumed for S_p.

According to McDonald, Lamki, and Delaney[2] an average of 12.7 low-energy electrons are emitted, per emission event, from a 2000 Å polycrystalline CsI photocathode (excited with 5.9-keV x rays). Henke, Knauer, and Premaratne have measured the ratio between the number of electrons ejected with energies above 50 eV to the total number of emitted electrons. They find a ratio of 1/100. (Data for the same ratio with 15 eV as an electron energy threshold are not available. However, because the majority of secondaries have energies less than 5 eV we expect the error in this estimate to be small compared to other estimates which will be discussed shortly.) Assuming (i) that electrons with energies above 50 eV are emitted with a $\cos^2\gamma$ distribution, where γ is the angle between the polarization vector and the momentum vector of the emitted electron,[27] (ii) that each ejected primary electron is not accompanied by any low-energy secondary electrons, and considering the opening angle of our detector we find that $\eta<1/40$. We note that both assumptions lead to an overestimate of η.

If we now take $M \leq 1.1\%$ from the upper limit of our experimental results, $\eta \leq 0.025$, and $M_p \leq 100\%$ (the maximum possible value) we find, using Eq. (23), that $M_s \leq 3.6\%$. We note that the use of Eq. (23) implicitly assumes that the difference between the phases of S_p and S_s is 90°. If the phases of S_p and S_s are assumed to be equal we find, using Eq. (22), $M_s \leq 1.1\%$, where we took $M_p=0$.

These limits on M_s are obtained under rather extreme assumptions. For example, the assumption $M_p=100\%$ can be realized only if all electrons with energies above 15 eV are emitted with a highly aspherical angular distribution. Our own data indicate that $M_p \leq 30\%$.[26] Using $M_p=30\%$, and assuming opposite phases, we obtain $M_s<1.9\%$.

An emission event is initiated when an x ray is absorbed and a primary electron is ejected from an atomic core level. Subsequent inelastic collisions create the low-energy secondary electrons. The angular distribution of the primary photoelectrons depends on the polarization of the exciting photon; the photoelectron is preferentially emitted in the direction of the polarization vector. Our results with CsI indicate that at most only a low level ($M_s<3.6\%$) of dependence on the initial polarization is retained in the number of emission events of low-energy electrons. This can be rephrased as implying that the probability for the emission of at least one low-energy electron [Y_{Ps} of Eq. (19)] is independent of the state of polarization of the exciting x-ray beam.

ACKNOWLEDGMENT

This work was supported in part by NASA Grant No. NAG5-618.

APPENDIX: INSTRUMENTAL MODULATION AND ELECTRON COLLECTION EFFICIENCY

1. Sources of instrumental modulation

In order to analyze the spurious modulation that may arise from an incomplete collection of electrons we find it useful to define the detection efficiency ϵ of the detector as the ratio of the number of electrons detected by the detector to the number of electrons emitted from the surface of the photocathode. We write[28]

$$\epsilon(\phi)=K\int f_e(r,\Theta,\Phi,E_e,\phi)f_d(r,\Theta,\Phi,E_e)dr\,d\Omega\,dE_e , \quad (A1)$$

where f_e is the probability density for the emission of an

electron at position r away from the axis of symmetry of the detector (assumed to have cylindrical symmetry), into a solid angle $d\Omega$ (Θ and Φ are the polar and azimuthal angles, respectively), and at an energy E_e. f_d is the probability density for the detection of an electron emitted with the same parameters. The variable r is introduced in order to account for the size of the projection of the beam on the photocathode. We recall that ϕ is the rotation angle of the photocathode-detector assembly around the z axis. The normalization factor K is given by

$$K = \left[\int f_e(r,\Theta,\Phi,E_e,\phi) dr\, d\Omega\, dE_e \right]^{-1} . \quad \text{(A2)}$$

Spurious modulation will arise if ϵ is a function of ϕ which varies sinusoidally with a 2ϕ dependence.

Since the detector is fixed with respect to the photocathode, f_d is independent of ϕ. f_e will, however, depend on ϕ if the x-ray beam is not collinear (parallel and coincident) with the axis of rotation of the photocathode, and because of the elongated projection of the beam on the photocathode.

If a pencil-like beam is displaced a distance d perpendicular to the axis of rotation of the photocathode, its trajectory on the photocathode surface, as it is rotated in the ϕ direction, will have an elliptical shape. The short axis of this ellipse is given by d and the long axis is given by $(d/\sin\theta)$, where θ is the grazing incidence angle of the beam on the photocathode. Such a trajectory of the beam on the photocathode plane will cause emission of electrons from different values of r, depending on ϕ, thus causing f_e to vary with ϕ.[29]

The extent of the projection of the beam on the photocathode, for a given angle ϕ, is determined by the size of the beam and by $\sin\theta$. Clearly, the size and shape of the projection will vary as the photocathode is turned in the ϕ direction. If the beam has a characteristic dimension t and is displaced by d from the axis of rotation of the photocathode, then photoelectrons may be emitted from the photocathode surface from locations which are either $\sim(d+t)$ or $\sim(d+t)/\sin\theta$ from the axis of rotation of the photocathode, depending on the angle ϕ.

Now, if the photoelectron detection radius is not much larger than $(d+t)/\sin\theta$, i.e., if $f_d \simeq 0$ for $r < (d+t)/\sin\theta$, then ϵ will be a function of ϕ and different count rates will result as a function of rotation in the ϕ direction. Such variation in the count rate will have a $\cos(2\phi)$ dependence resulting in spurious modulation and the occurrence of arbitrary "phase shifts" in the rotation curves. Also, different pulse-height distributions will be recorded at different polarization states. An experimental demonstration of these effects is presented elsewhere.[26]

To perform a valid experiment these problems must be minimized by a precise alignment of the x-ray beam with the axis of rotation, by utilizing a beam with a small cross section, and by enlarging the detection radius of the detector.

In the experiment presented here, the axis of rotation was first determined experimentally by means of a laser beam. After the laser beam traced the axis of rotation, two circular collimators, 1.6 mm in diameter each, were placed along this beam between the Bragg crystal and the photocathode so as to define the axis of rotation mechanically. The collimators serve not only to define the axis of rotation but also to confine the beam size and determine its shape. We measured the beam's cross section and found that the beam was 1.5 and 1.8 mm wide in the x and y directions, respectively. Combining the projection of such a beam on the photocathode, at a grazing incidence angle of 10° (5°), with the maximal possible displacement of the center of the beam from the axis of rotation, we find that emission of electrons is contained to a radius of 9 mm (18 mm) from the axis of rotation.

2. Electron collection efficiency

To test experimentally the electron collection efficiency of our electron optics system we measured the count rate as a function of grid No. 1 potential (see Fig. 2), with the field forming ring potential, grid No. 2 potential, and the entrance aperture of the MCP potential fixed at 0, +480, and +500 V, respectively. The potential of grid No. 1 was varied between 0 and +500 V. One expects that as grid No. 1 potential is increased, more electrons will be focused into the detector resulting in an increase in the count rate. Saturation of the count rate indicates that a sufficient number of electrons are collected such that essentially all the emission events which contain low-energy electrons are recorded. This is because the energy distribution of the low-energy electrons is a smooth function and the probability for emission of electrons of energy higher than 15 eV is essentially negligible.[1] The experiment was conducted at a grazing incidence angle of 5°, where the spread of the beam on the photocathode is largest, and at two polarization states, σ and π.

We found that, at both polarization states, count rates at grid No. 1 potentials larger than 50 V did not increase by more than 0.5% compared to the count rate recorded at 50 V. Saturation was observed at relatively low focusing voltages. This is because the electronic emission from CsI is dominated by very-low-energy electrons.

We conclude that more than 99.5% of the events which contain low-energy electrons are detected at both polarization states, and that instrumental spurious modulation due to incomplete detection of events is limited to less than 0.25%.

---

*Present address: Instituto di Fisica Cosmica ed Applicazioni dell' Informatica/CNR, via M. Stabile 172, 90139 Palermo, Italy.

[1]B. L. Henke, J. P. Knauer, and K. Premaratne, J. Appl. Phys. **52**, 1509 (1981).

[2]I. R. McDonald, A. M. Lamki, and C. F. G. Delaney, J. Phys. D **6**, 87 (1973).

[3]See, for example, L. G. Eliseenko, V. N. Shchemelev, and M. A. Rumsh, Zh. Tekh. Fiz. **38**, 175 (1968) [Sov. Phys. Tech. Phys. **13**, 122 (1968)].

[4]*Particle Induced Electron Emission I, II,* edited by G. Höhler, *Springer Tracts in Modern Physics,* Vols. 122, 123 (Springer-

Verlag, Berlin, 1991).
[5]J. Elster and H. Geitel, Ann. Phys. (N.Y.) **52**, 433 (1894); **55**, 684 (1895); **61**, 445 (1895).
[6]H. E. Ives, Phys. Rev. **38**, 1209 (1931).
[7]J. Monin and G. A. Boutry, Phys. Rev. B **9**, 1309 (1974).
[8]J. K. Sass, H. Laucht, and K. L. Kliewer, Phys. Rev. Lett. **35**, 1461 (1975).
[9]S. A. Flodström and J. G. Endriz, Phys. Rev. B **12**, 1252 (1975).
[10]H. Petersen and S. B. M. Hagström, Phys. Rev. Lett. **41**, 1314 (1978).
[11]G. Jezequel, Phys. Rev. Lett. **45**, 1963 (1980).
[12]P. Zetner, A. Pradhan, W. B. Westerveld, and J. W. McConkey, Appl. Opt. **22**, 2210 (1983).
[13]R. M. Broudy, Phys. Rev. B **3**, 3641 (1971), and references therein.
[14]S. A. Flodström and J. G. Endriz, Phys. Rev. B **31**, 893 (1973), and references therein.
[15]M. A. Rumsh and V. N. Shchemelev, Fiz. Tverd. Tela (Leningrad) **4**, 2050 (1963) [Sov. Phys. Solid State **4**, 1503 (1963)].
[16]A. L. Morse, Ph.D. thesis, University of Southern California, 1968.
[17]G. W. Fraser, J. E. Lees, and J. F. Pearson, Nucl. Instrum. Methods **A284**, 483 (1989).
[18]G. W. Fraser, M. D. Pain, J. F. Pearson, J. E. Lees, C. R. Binns, P. S. Shaw, and J. R. Fleischman, SPIE Proc. **1548**, 132 (1991).
[19]P. S. Shaw, E. D. Church, S. Hanany, Y. Liu, J. Fleischman, P. Kaaret, and R. Novick, SPIE Proc. **1343**, 485 (1990).
[20]P. Kaaret, R. Novick, A. Heckler, P. Shaw, G. W. Fraser, J. E. Lees, and J. F. Pearson, in *High Energy Astrophysics in the 21st Century,* edited by C. Joss, AIP Conf. Proc. No. 211 (AIP, New York, 1989), p. 120.
[21]A. Heckler, A. Blaer, P. Kaaret, and R. Novick, SPIE Proceedings **1160**, 580 (1989).
[22]The simulations were done with a program developed by W. B. Herrmannsfeldt. See W. B. Herrmannsfeldt, in *Linear Accelerator and Beam Optics Codes Workshop,* edited by C. R. Eminhizer, AIP Conf. Proc. No. 177 (AIP, New York, 1988), p. 45; W. B. Herrmannsfeldt, R. Becker, I. Brodie, A. Rosengreen, and C. A. Spindt, Nucl. Instrum. Methods **A298**, 39 (1990).
[23]G. W. Fraser, Nucl. Instrum. Methods **206**, 265 (1983).
[24]K. Premaratne, E. R. Dietz, and B. L. Henke, Nucl. Instrum. Methods **207**, 465 (1983).
[25]J. H. Chappel, E. Everman, and S. S. Murray, Nucl. Instrum. Methods **A260**, 483 (1987).
[26]S. Hanany, Ph.D. thesis, Columbia University, 1993.
[27]For simplicity we are using the differential photoionization cross section of a K shell in the dipole approximation. The angular distribution of all electrons with energies more than 50 eV is expected to be less aspherical, making our value of η an overestimate.
[28]Equation (A1) is valid for detection of single electrons. Although in our experiment we detect emission *events* rather than single electrons, the arguments that show the origin of the spurious effects are not affected by this difference.
[29]Angular misalignment and its combination with translational displacement is analyzed elsewhere (Ref. 26). We show that an angular misalignment may cause the count rate to depend on ϕ (and not on 2ϕ).